

Single laser-pulse implementation of arbitrary ZYZ rotations of an atomic qubit

Han-gyeol Lee, Yunheung Song, and Jaewook Ahn*
Department of Physics, KAIST, Daejeon 305-701, Korea

Arbitrary rotation of a qubit can be performed with a three-pulse sequence; for example, ZYZ rotations. However, this requires precise control of the relative phase and timing between the pulses, making it technically challenging in optical implementation in a short time scale. Here we show any ZYZ rotations can be implemented with a single laser-pulse, that is *a chirped pulse with a temporal hole*. The hole of this shaped pulse induces a non-adiabatic interaction in the middle of the adiabatic evolution of the chirped pulse, converting the central part of an otherwise simple Z-rotation to a Y rotation, constructing ZYZ rotations. The result of our experiment performed with shaped femtosecond laser pulses and cold rubidium atoms shows strong agreement with the theory.

PACS numbers: 32.80.Qk, 42.50.Dv, 42.50.Ex

I. INTRODUCTION

Qubit is the information stored in the quantum state of a two-level system, routinely used as the smallest unit of information processed in the quantum circuit model of quantum computation [1]. In order to construct a universal computational gate set, single-qubit rotations, about at least two distinct rotational axes are required as well as a two-qubit gate, e.g., the CNOT gate. Single-qubit rotation gates, such as Hadamard and Pauli X, Y, and Z gates have been implemented on numerous physical systems, including photons [2], ions [3], atoms [4], molecules [5], quantum dots [6], and superconducting qubits [7].

Many single-qubit rotations in a sequence can also be performed with *a single arbitrary rotation gate*, which simplifies otherwise complex physical implementation of many distinct rotations in a unified fashion. An arbitrary rotation (of rotation angle ϕ and rotational axis \hat{n}) can be constructed with a minimum of three rotations that correspond to the set of Euler angle rotations: for example, the three rotations in the best-known ZYZ-decomposition are given by

$$\mathcal{R}_{\hat{n}}(\phi) = \mathcal{R}_{\hat{z}}(\Phi_2)\mathcal{R}_{\hat{y}}(\Theta)\mathcal{R}_{\hat{z}}(\Phi_1), \quad (1)$$

where \mathcal{R} represents a rotational transformation, and \hat{n} and ϕ are respectively given as a function of three rotation angles Φ_1 , Φ_2 , and Θ [8]. In an optical implementation of two-level system dynamics, Z-rotations use either a time-evolution or a far-detuned excitation [9, 10], and X or Y-rotations a resonant area-pulse interaction, both of which and their combinations require a precise control of the relative phase and timing among the constituent pulsed interactions.

In this paper, we show that an arbitrary rotation can be, alternatively, performed with a single laser-pulse, when the pulse is programmed to be *a chirped pulse with a temporal hole*. As to be discussed in the rest of the paper, a single laser pulse with the given pulse shape implements ZYZ-decomposed rotations all at once, where the

temporal hole in the middle of a chirped pulse induces a strong non-adiabatic evolution, which is a Y-rotation, amid an otherwise monotonic adiabatic evolution, a Z-rotation, due to the chirped pulse. The predicted behavior of the ZYZ-decomposition is to be experimentally verified with cold atomic qubits and as-programmed femtosecond laser pulses.

II. THEORETICAL ANALYSIS

We consider the dynamics of a two-level atom, driven by a chirped laser pulse with a temporal hole. The electric field of the pulse, where both the main pulse and the hole are assumed to be of Gaussian pulse shape, is given by

$$E(t) = E_0(e^{-t^2/\tau^2} - ke^{-t^2/\tau_h^2}) \cos(\omega_0 t + \alpha t^2 + \varphi), \quad (2)$$

where τ and τ_h are respectively the widths of the main pulse and the hole, k ($0 \leq k \leq 1$) is the depth of the hole, α is the linear chirp parameter, and φ is the carrier phase. The contribution of the carrier phase is a simple Z-rotation, *i.e.* $\mathcal{R}_{\hat{z}}(\varphi)$, so we will first consider the $\varphi = 0$ case. When the state vectors are defined by $|g\rangle$ and $|e\rangle$ (of respective energies 0 and $\hbar\omega_0$), the interaction Hamiltonian in the adiabatic basis [11, 12], after the rotating wave approximation, is given by

$$H = \frac{\hbar}{2} \begin{bmatrix} \lambda_- & -2i\dot{\vartheta} \\ 2i\dot{\vartheta} & \lambda_+ \end{bmatrix}, \quad (3)$$

where $\lambda_{\pm} = \pm\sqrt{\Omega^2 + \Delta^2}$ are the eigenvalues in the bare basis, for the Rabi frequency Ω and the instantaneous detuning $\Delta = -2\alpha t$, and ϑ is the adiabatic mixing angle defined by $2\vartheta = \tan^{-1}\Omega/\Delta$ for $0 \leq \vartheta \leq \pi/2$. However, with Eq. (3), the phase of the state diverges at $t \rightarrow \pm\infty$, so we use an additional transformation $\exp\left(i\int_0^t T_{\Delta} dt'/\hbar\right)$ with $T_{\Delta} = \frac{\hbar}{2} \begin{bmatrix} -|\Delta| & 0 \\ 0 & |\Delta| \end{bmatrix}$ to remove this rapidly oscillating phase. The resulting Hamiltonian is given in the interaction picture by

$$H' = \frac{\hbar}{2} \begin{bmatrix} |\Delta| - \sqrt{\Delta^2 + \Omega^2} & -2i\dot{\vartheta}e^{-i|\Delta|/2} \\ 2i\dot{\vartheta}e^{i|\Delta|/2} & \sqrt{\Delta^2 + \Omega^2} - |\Delta| \end{bmatrix}. \quad (4)$$

*Electronic address: jwahn@kaist.ac.kr

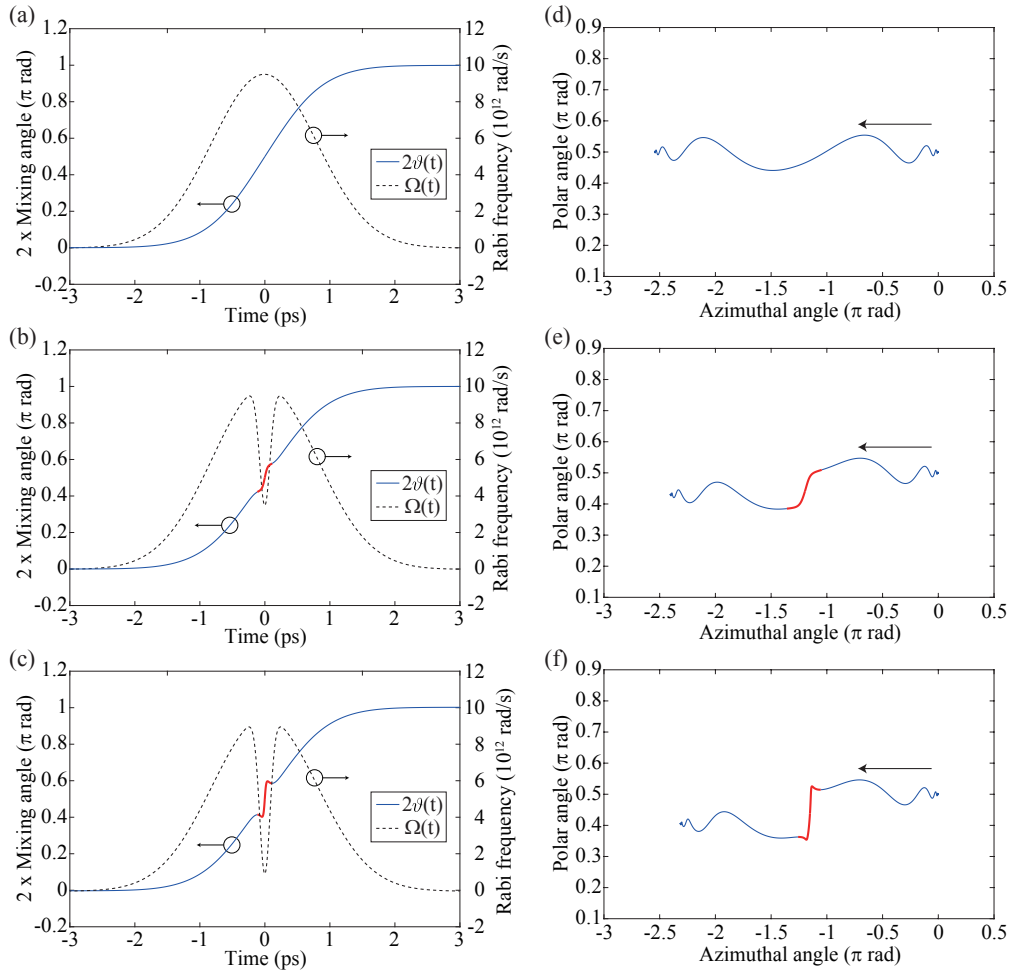


FIG. 1: (Color online) (a-c) Time dependence of Rabi frequency Ω and mixing angle 2ϑ plotted for (a) a chirped pulse, (b) a chirped pulse with a temporal hole of width $\tau_h = 0.1\tau$ and depth $k = 0.9$, and (c) of $\tau_h = 0.1\tau$ and $k = 1$. (d-f) Bloch vector evolution in the adiabatic basis corresponding to (a), (b), and (c), where the x -axis is the azimuth angle of the Bloch sphere and the y -axis is the polar angle. The thick red lines in (b), (c), (e) and (f) indicate the $-\tau_h < t < \tau_h$ region (see text).

Figure 1 shows the behavior of the mixing angle ϑ , compared with the Rabi frequency Ω for various hole depth k (left panel), and the corresponding Bloch vector evolution (right panel). The pulse without a hole in Fig. 1(a) shows a slow change in ϑ and relatively large Ω , suggesting that the adiabatic condition, $2\dot{\vartheta} \ll |\lambda_+ - \lambda_-|$, is satisfied in all time. So, a pulse without a hole induces an adiabatic evolution, *i.e.* a Z-rotation in the adiabatic basis, as depicted in Fig. 1(d).

On the other hand, the pulses with a hole in Figs. 1(b) and 1(c) exhibit an abrupt change in ϑ near $t = 0$. Therefore, the overall dynamics may be decomposed to three sub-dynamics in different time zones: $t < -\tau_h$, $-\tau_h < t < \tau_h$, and $t > \tau_h$, as clearly shown in Figs. 1(e) and 1(f). In the central time zone ($-\tau_h < t < \tau_h$), the hole makes Ω small and a rapid change in ϑ occurs. Since the Hamiltonian is dominated by the non-adiabatic coupling in the off-diagonal components, it is approximately

given by

$$H'(t \approx 0) \approx \frac{\hbar}{2} \begin{bmatrix} 0 & -2i\dot{\vartheta} \\ 2i\dot{\vartheta} & 0 \end{bmatrix}, \quad (5)$$

which corresponds to a Y-rotation with a rotation angle

$$\Theta = \int_{-\tau_h}^{\tau_h} 2\dot{\vartheta} dt = 2[\vartheta(\tau_h) - \vartheta(-\tau_h)]. \quad (6)$$

In both side regions ($t < -\tau_h$ and $t > \tau_h$), Z-rotations occur due to the adiabatic evolution of the chirped pulse. The rotation angles are respectively given by

$$\Phi_1 = \int_{-\infty}^{-\tau_h} [|\Delta(t)| - \sqrt{\Delta^2(t) + \Omega^2(t)}] dt \quad (7)$$

$$\Phi_2 = \int_{\tau_h}^{\infty} [|\Delta(t)| - \sqrt{\Delta^2(t) + \Omega^2(t)}] dt, \quad (8)$$

and when there is no detuning [13], Φ_1 equals Φ_2 due to the symmetry. As a result, the total time-evolution,

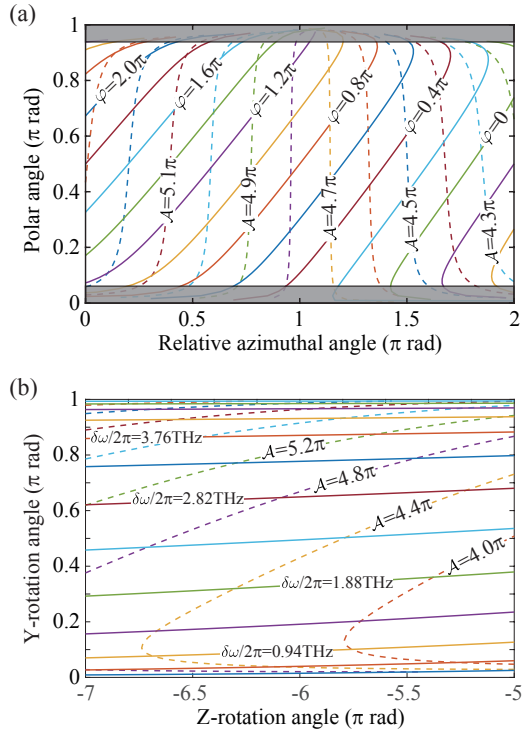


FIG. 2: (Color online) (a) Final states on the Bloch sphere spanned by the interaction of the chirped pulse with a temporal hole, for an initial state $(|g\rangle + |e\rangle)/\sqrt{2}$. The pulse carrier-envelope phase φ and the equivalent pulse-area \mathcal{A} [14] were varied, while $\tau = 5.9$ ps, $\alpha = 1.25$ rad/ps², $\tau_h = 0.5\tau$, and $k = 0.95$ were kept constant. Note that the shaded regions near the poles are physically unfeasible, requiring extreme conditions. (b) Estimated Z- and Y-rotation angles, Φ_2 and Θ , spanned by varying \mathcal{A} and $\delta\omega$ (detuning) [13], while $\tau = 2.95$ ps, $\alpha = 2.5$ rad/ps², $\tau_h = 0.5\tau$ and $k = 0.7$ were fixed.

including the Z-rotation due to the carrier phase $\mathcal{R}_z(\varphi)$, is given by

$$\mathcal{R}_z(\Phi_2)\mathcal{R}_y(\Theta)\mathcal{R}_z(\Phi_1 + \varphi) = \begin{bmatrix} e^{-i(\Phi_1 + \Phi_2 + \varphi)/2} \cos \frac{\Theta}{2} & -e^{i\varphi/2} \sin \frac{\Theta}{2} \\ e^{-i\varphi/2} \sin \frac{\Theta}{2} & e^{i(\varphi + \Phi_1 + \Phi_2)/2} \cos \frac{\Theta}{2} \end{bmatrix}, \quad (9)$$

which corresponds to ZYZ rotations.

When the qubit starts from an initial state defined by

$$|\psi_{\text{init}}\rangle = \frac{1}{\sqrt{2}} (|g\rangle + |e\rangle), \quad (10)$$

it can go, through the interaction with the as-programmed laser pulses, to an arbitrary position on the Bloch sphere, as shown in Fig. 2(a). While this is only true for certain initial qubit states, as $\Phi_{1,2}$ and Θ in Eq. (9) are not fully independent, the rotations can be made arbitrary: by using the detuning and pulse area in Eq. (2), the full range range 2π for Φ_2 and π for Θ are completely spanned as in Fig. 2(b), ensuring the given ZYZ rotations to be arbitrary.

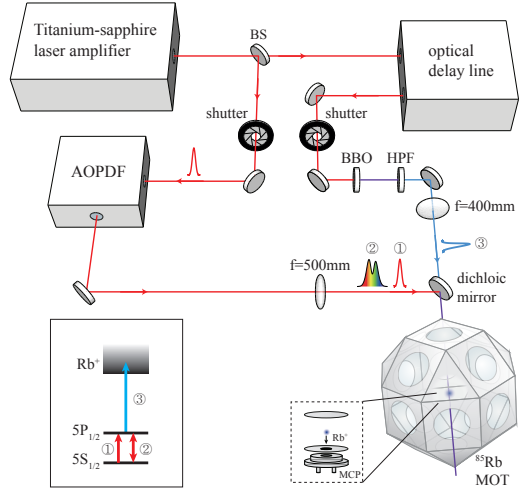


FIG. 3: (Color online) Schematic of the experimental setup: Laser pulses were from the femtosecond laser and programmed to operate arbitrary single qubit rotations of cold atom qubits in a magneto-optical trap. Inset shows the energy level structure of the atomic qubit along with ionization states. The arrows labeled with numbers illustrate the experimental pulse sequence.

III. EXPERIMENTAL VERIFICATION

In order to verify the ZYZ rotations, of the chirped pulse with a temporal hole, we performed a proof-of-principle experiment with cold atomic qubits and as-programmed femtosecond laser pulses (see Fig. 3). The detail of our laser experimental setup was described in our previous work [15, 16]. Briefly, we used amplified optical pulses from a Ti:sapphire mode-locked laser. Initial pulses were produced at a repetition rate of 1 kHz from the laser, wavelength-centered at the resonance wavelength 795 nm of the rubidium transition from $5S_{1/2}$ to $5P_{1/2}$. The spectral bandwidth was 2.5 THz in Gaussian width, equivalent to a pulse duration of 212 fs (FWHM) for a transform-limited Gaussian pulse. The pulses were then shaped with an acousto-optic pulse programming device (AOPDF, Dazzler from Fastlite) [17]. The two-level system was formed with the ground and excited states, $|g\rangle = 5S_{1/2}$ and $|e\rangle = 5P_{1/2}$, of atomic rubidium (^{87}Rb) and the atoms were held in a magneto-optical trap [9]. The inhomogeneity of the laser-atom interaction [18], due to the spatial intensity profile of the laser, was minimized by reducing the size of the atom cloud 2.3 times smaller than the the laser beam size. The size of the atom cloud was 250 μm (FWHM).

The control experiment was conducted in three steps: initialization, qubit rotation, and detection. The atoms were first excited by a $\pi/2$ -area pulse to initialize the atoms in the superposition state $|\psi_{\text{init}}\rangle$ defined in Eq. (10). Then, the chirped pulse with a temporal hole performed a rotation of the atomic state, $|\psi\rangle =$

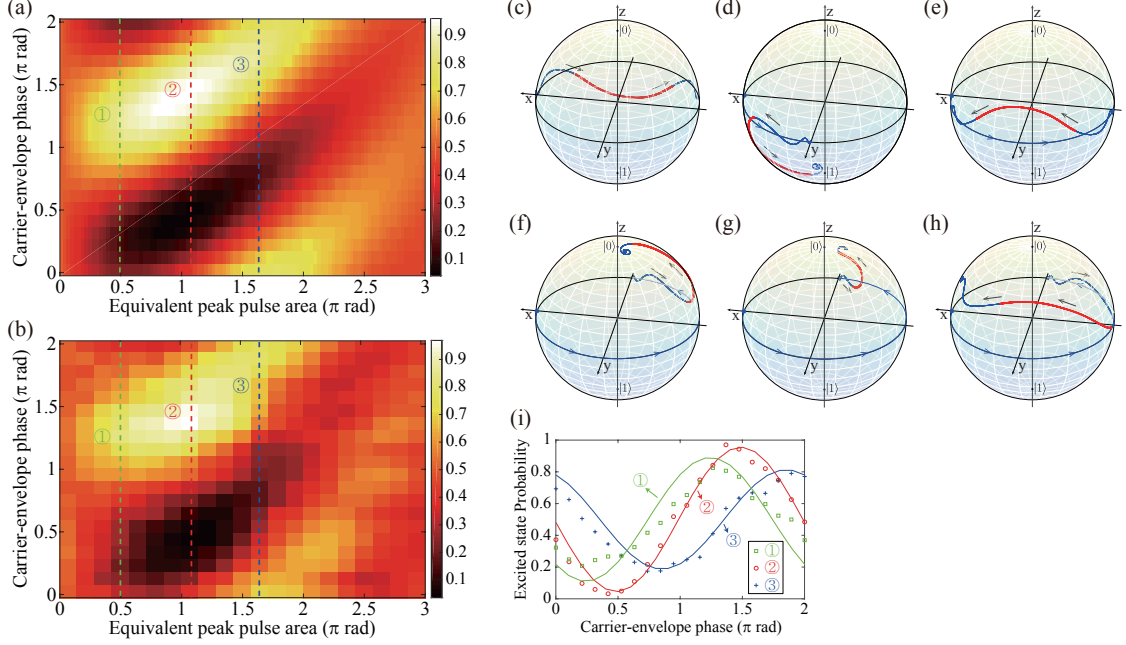


FIG. 4: (Color online) (a) Measured excitation probability $P_e(\Theta, \varphi, \Phi_1)$, of atoms initially in $|\psi_{\text{init}}\rangle = (|g\rangle + |e\rangle)/\sqrt{2}$, probed as a function of the equivalent pulse-area \mathcal{A} [14] and the carrier phase φ , where the chirped pulse with a temporal hole is defined in Eq. (2) with $k = 0.7$. (b) The corresponding TDSE calculation. (c-h) Bloch vector dynamics at selected points: (c) $(\varphi, \mathcal{A}) = (0, \pi)$, (d) $(\pi/2, \pi)$, (e) (π, π) , (f) $(3\pi/2, \pi)$, (g) $(3\pi/2, \pi/2)$, (h) $(3\pi/2, 3\pi/2)$. (i) Comparison between the experimental results and calculation along the three dashed lines in (a) and (b).

$\mathcal{R}_z(\Phi_1)\mathcal{R}_y(\Theta)\mathcal{R}_z(\Phi_1 + \varphi)|\psi_{\text{init}}\rangle$. Lastly, atoms in the excited state were detected through ionization, using a frequency-doubled split-off of an un-shaped laser pulse and a micro-channel plate (MCP) detector.

The laser pulses for the initialization and qubit rotation were programmed, with a fixed relative phase, by the AOPDF. In the frequency domain, the combined field is given by

$$\tilde{E}(\omega) = \tilde{E}_{\text{init}}(\omega) + \tilde{E}_{\text{rot}}(\omega)e^{i\varphi}, \quad (11)$$

where $\tilde{E}_{\text{init}}(\omega)$ is the $\pi/2$ -area pulse, $\tilde{E}_{\text{rot}}(\omega)$ is the chirped pulse with a temporal hole, and φ is the carrier phase of the rotation pulse relative to the initialization pulse. The total energy of these two pulses was up to 20 μJ and the energy of each pulse was pre-calibrated through cross-correlation measurements. The chirp parameter for the control pulse was fixed at $\alpha = 8.15 \text{ rad}/\text{ps}^2$, which corresponds to frequency chirp of 60,000 fs^2 in the spectral domain.

Figure 4 shows a comparison between experimental and theoretical results. When atoms, in the initial superposition state $|\psi_{\text{init}}\rangle$ in Eq. (10), undergo the rotation, given in Eq. (9), the excited-state probability is given by

$$\begin{aligned} P_e(\Theta, \varphi, \Phi_1) &= |\langle e | \mathcal{R}_z(\Phi_2)\mathcal{R}_y(\Theta)\mathcal{R}_z(\Phi_1 + \varphi) | \psi_{\text{init}} \rangle|^2 \\ &= \frac{1}{2} [1 + \sin \Theta \cos(\Phi_1 + \varphi)]. \end{aligned} \quad (12)$$

The resulting behavior of P_e is an oscillatory function, of which the amplitude and phase are determined by Θ and

$\Phi_1 + \varphi$. In Fig. 4(a), the measured probability is plotted as a function of the equivalent (peak) pulse-area [14] and the carrier phase φ . The result strongly agrees with the calculation in Fig. 4(b), performed with the corresponding time-domain Schrödinger equation (TDSE). Each point in Figs. 4(a) and 4(b) corresponds to a distinct Bloch vector evolution. A few characteristic trajectories are shown in Figs. 4(c,d,⋯,h) (see the figure caption for more detail).

Along the dashed lines in Figs. 4(a) and 4(b), data points are extracted and compared in Fig. 4(i), where the excited-state probabilities, $P_e(\varphi|\Theta, \Phi_1)$, are plotted as a function of φ at fixed Θ and Φ_1 . The change of the peak oscillation point in Fig. 4(i) is related to the E_0 -dependence of Φ_1 as in Eq. (12); Φ_1 is a monotonically decreasing function of E_0 , so the peaks in Fig. 4(i) shift to the upper right corner as E_0 increases. Also, the change in the oscillation amplitude is related to the E_0 -dependence of Θ . As the electric-field amplitude E_0 increases, so does the rotation angle Θ of the Y-rotation; however, it is up to a certain maximum E_0 , at above of which the dynamics involved with the hole gradually becomes adiabatic. Such behavior of Θ is clearly demonstrated in Fig. 4(i), where the oscillation amplitude given by $\sin \Theta$ in Eq. (12) reaches maximal, along the line marked by ②, and decreases as E_0 increases. Therefore, the expected behavior Φ_1 and Θ in Eq. (12) is clearly observed in the experimental results.

IV. CONCLUSION

In summary, we proposed and demonstrated the use of hybrid adiabatic and non-adiabatic interaction for single laser-pulse implementation of arbitrary qubit rotations. The chirped optical pulse with a temporal hole induced ZYZ-decomposed rotations of atomic qubits all at once, in which the temporal hole caused a non-adiabatic evolution amid an otherwise monotonic adiabatic evolution due to the chirped pulse. The proof-of-principle experimental verification of the given laser-atom interaction was performed with programmed femtosecond laser

pulses and cold atoms. The result suggests that laser pulse-shape programming may be useful in quantum computation through concatenating gate operations in a quantum circuit.

Acknowledgments

This research was supported by Samsung Science and Technology Foundation [SSTF-BA1301-12]. Authors thank Adam Massey and Chansuk Park for fruitful discussions.

-
- [1] M. A. Nielsen and I. L. Chuang, *Quantum Computation and Quantum Information* (Cambridge University Press, 2000).
- [2] P. Kok, W. J. Munro, K. Nemoto, T. C. Ralph, J. P. Dowling, and G. J. Milburn, *Rev. Mod. Phys.* **79**, 135 (2007).
- [3] H. Häffner, C. F. Roos, and R. Blatt, “Quantum computing with trapped ions,” *Phys. Rep.* **469**, 155 (2008).
- [4] M. Saffman, “Quantum computing with atomic qubits and Rydberg interactions: progress and challenges,” *J. Phys. B* **49**, 202001 (2016).
- [5] R. Hildner, D. Brinks, and N. F. van Hulst, “Femtosecond coherence and quantum control of single molecules at room temperature,” *Nat. Phys.* **7**, 172 (2011).
- [6] F. H. L. Koppens, C. Buiszert, K. J. Tielrooij, I. T. Vink, K. C. Nowack, T. Meunier, L. P. Kouwenhoven, and L. M. K. Vandersypen, “Driven coherent oscillations of a single electron spin in a quantum dot,” *Nature* **442**, 766 (2006).
- [7] E. Lucero, M. Hofheinz, M. Ansmann, R. C. Bialczak, N. Katz, M. Neeley, A. D. O’Connell, H. Wang, A. N. Cleland, and J. M. Martinis, “High-fidelity gates in a single Josephson qubit,” *Phys. Rev. Lett.* **100**, 247001 (2008).
- [8] The rotational axis and angle of a ZYZ-decomposed arbitrary rotation are respectively given by $\hat{n} = (\sin \frac{\Theta}{2} \sin \Phi_+, \sin \frac{\Theta}{2} \cos \Phi_-, \cos \frac{\Theta}{2} \sin \Phi_+)/\sin \frac{\phi}{2}$ and $\phi = 2 \cos^{-1}(\cos \frac{\Theta}{2} \cos \Phi_+)$, where $\Phi_{\pm} = (\Phi_1 \pm \Phi_2)/2$.
- [9] J. Lim, H. G. Lee, S. Lee, C. Y. Park, and J. Ahn, “Ultrafast Ramsey interferometry to implement cold atomic qubit gates,” *Sci. Rep.* **4**, 5867 (2014).
- [10] Y. Wang, A. Kumar, T.-Y. Wu, and D. S. Weiss, “Single-qubit gates based on targeted phase shifts in a 3D neutral atom array,” *Science* **352**, 1562 (2016).
- [11] B. W. Shore, *Manipulating Quantum Structures Using Laser Pulses* (Cambridge University Press, 2011).
- [12] L. Allen and J. H. Eberly, *Optical Resonance and Two-Level Atoms* (Dover, 1987).
- [13] When the hole is at $t = 0$, detuning $\delta\omega$ is implemented by time shift $\delta t \simeq \delta\omega/2\alpha$. The electric field is then given by $E(t) = E_0[e^{-(t-\delta t)^2/\tau^2} - ke^{-\delta t^2/\tau^2} e^{-t^2/\tau_h^2} \cos(\omega_0 t + \alpha t^2)]$.
- [14] Equivalent pulse-area \mathcal{A} is defined by the pulse area of an equivalent transform-limited pulse with the same pulse energy and bandwidth.
- [15] H. G. Lee, Y. Song, H. Kim, H. Jo, and J. Ahn, “Quantum dynamics of a two-state system induced by a chirped zero-area pulse,” *Phys. Rev. A* **93**, 023423 (2016).
- [16] Y. Song, H. G. Lee, H. Jo, and J. Ahn, “Selective excitation in a three-state system using a hybrid adiabatic-nonadiabatic interaction,” *Phys. Rev. A* **94**, 023412 (2016).
- [17] P. Tournois, “Acousto-optic programmable dispersive filter for adaptive compensation of group delay time dispersion in laser systems,” *Opt. Comm.* **140**, 245 (1997).
- [18] H. G. Lee, H. Kim, and J. Ahn, “Ultrafast laser-driven Rabi oscillations of a Gaussian atom ensemble,” *Opt. Lett.* **40**, 510 (2015).